An Optically Transparent Focused P(VDF-TrFE) Transducer for Photoacoustic Microscopy (PAM)

Cheng Fang, *Graduate Student Member, IEEE*, Zijie Zhao, Jie Fang, and Jun Zou, *Senior Member, IEEE*

***Abstract*—This article reports a new optically transparent focused poly(vinylidene fluoride-co-trifluoroethylene) [P(VDF-TrFE)] transducer for photoacoustic microscopy (PAM), which is fabricated by a new process based on precutting and direct lamination. Compared with the previous fabrication process, it is simpler and makes it possible to achieve a high numerical aperture (NA) without stretching the (brittle) piezoelectric film. For demonstration, a prototype transducer has been fabricated with a 10-μm-thick 70/30 P(VDF-TrFE) film laminated onto a plano-concave glass lens with an acoustic NA of 0.64. Experimental characterizations show that the transducer has an optical transmittance of 88.6% (@ 532 nm) and an acoustic center frequency and −3-dB bandwidth (BW) of 24 and 29 MHz, respectively. Using the new optically transparent focused P(VDF-TrFE) transducer, a PAM setup has been built to carry imaging experiments on different targets. Based on the experimental results, it can be concluded that the optically transparent focused P(VDF-TrFE) transducer could be useful for the development of new PAM systems for different imaging applications.**

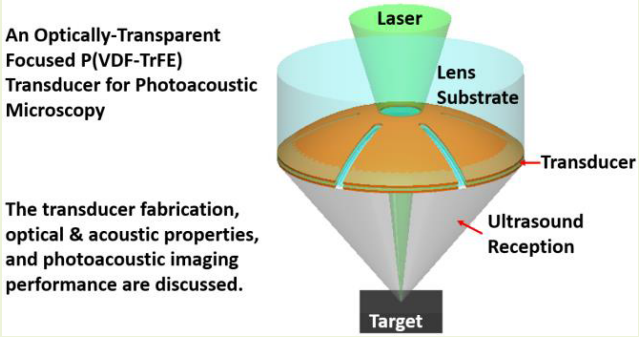

***Index Terms*—Optically transparent focused transducer, poly(vinylidene fluoride-co-trifluoroethylene) [P(VDF-TrFE)], photoacoustic microscopy (PAM).**

I. Introduction

As a unique hybrid imaging modality, photoacoustic microscopy (PAM) brings rich optical contrast at penetration depths beyond the optical diffraction limit in soft tissues [1], [2]. For PAM, efficient optical delivery and acoustic detection are necessary to achieve optimal imaging performance. Nevertheless, in current PAM systems, the optical and acoustic components may not be well compatible with each other. For instance, the (opaque) acoustic transducers could impede the light propagation onto the target, while the (glass) optical components hinder the induced photoacoustic (PA) signals from arriving at the transducer. To solve this problem, a variety of optically transparent transducers have been developed, including piezoelectric [3], [4], [5], capacitive [6], and even optical [7], [8], [9], [10] ones, each of which has its own advantages and disadvantages [11], [12]. By making the transducer optically transparent, new compact PAM configurations with easier alignment of the optical and acoustic beams can be achieved.

Among all optically transparent transducers developed so far, the focused polyvinylidene fluoride (PVDF) transducer [11], [12] is unique, due to its good optical transmittance, low acoustic impedance, broad acoustic bandwidth (BW), and outstanding shape-focusing capability with high numerical aperture (NA). Nevertheless, focused PVDF transducers have not been explored as widely as the lithium niobite ($LiNbO_3$) ones for in vivo imaging, which is mainly due to the more challenging fabrication process. The focused PVDF transducer is fabricated by a stretch-molding and transfer-bonding method (Fig. 1), which requires the substrates to be mechanically flexible with high stretchability (e.g., PVDF) and therefore cannot be applied onto other more rigid or brittle piezoelectric films. What is more, because the transducer has to be produced one by one, it is difficult to scale up for mass fabrication.

To address these issues, we have investigated a new fabrication process based on precutting and direct lamination, which eliminates the need of stretch molding and therefore is compatible even with nonstretchable piezoelectric films. With fewer steps, it is also possible to scale up for

Manuscript received 21 February 2023; revised 25 March 2023; accepted 1 May 2023. Date of publication 10 May 2023; date of current version 14 June 2023. This work was supported in part by the National Science Foundation under Grant 1748161. The associate editor coordinating the review of this article and approving it for publication was Prof. Sheng-Shian Li. *(Corresponding author: Jun Zou.)*

This work involved animals in its research. Approval of all ethical and experimental procedures and protocols was granted by the University Laboratory Animal Care Committee of Texas A&M University.

The authors are with the Department of Electrical and Computer Engineering, Texas A&M University, College Station, TX 77843 USA (e-mail: fangchengok2007@tamu.edu; zhao0013@tamu.edu; fangjie@tamu.edu; junzou@tamu.edu).

Digital Object Identifier 10.1109/JSEN.2023.3273554

TABLE I
RELEVANT MATERIAL PROPERTIES OF PVDF AND P(VDF-TRFE)

	Young's Modulus Y (GPa) [13] [14]	Acoustic Impedance Z (MRayl) [15] [16]	Density ρ (kg/m^3) [15]	Piezoelectric Coefficient d_{33} (pC/N) [17] [18] [19] [20]	Electromechanical coupling factor k_{33} [15] [17]	Dielectric loss tanδ [15]
PVDF	2.7	3.9-4.2	1,780	15-33	0.14-0.2	0.25
P(VDF-TrFE)	1.5	4.5	1,880	17.8-36	0.23-0.3	0.15

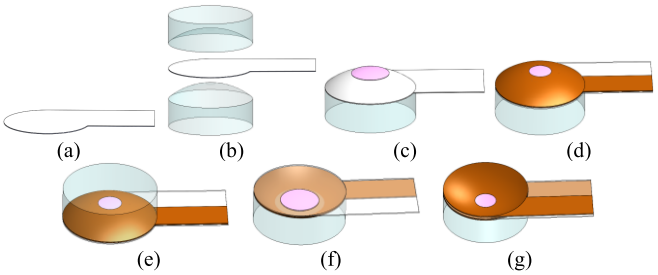

Fig. 1. Schematic of the stretch-molding and transfer-bonding process flow of the focused PVDF transducer. (a) and (b) Flat PVDF film molded and stretched by a pair of lenses. (c) and (d) Electrodes deposition on one side of PVDF. (e) PVDF bonded with concave lens and then convex lens released. (f) and (g) Electrodes deposition on the other side of PVDF.

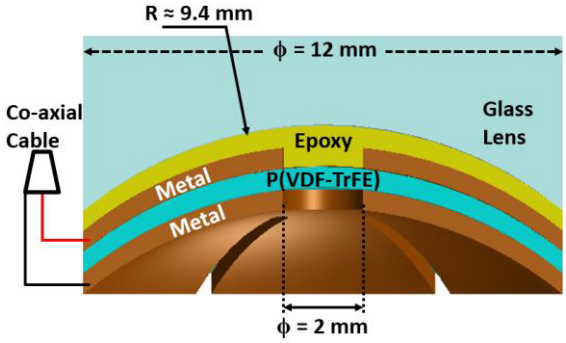

Fig. 2. Schematic cross-sectional design of the optically transparent focused P(VDF-TrFE) transducer.

mass fabrication. Based on this approach, a new high-NA optically transparent focused poly(vinylidene fluoride-co-trifluoroethylene) [P(VDF-TrFE)] transducer has been successfully fabricated and characterized. As shown in Table I, P(VDF-TrFE) is generally considered as a better substitute for PVDF [21]. However, because of its much lower mechanical flexibility and stretchability, it cannot be processed with the previous stretch-molding and transfer-bonding method. With the new optically transparent focused P(VDF-TrFE) transducer, a PAM imaging setup has been built to carry imaging experiments on different targets. Based on the experimental results, it can be concluded that compared with the previous PVDF transducer, the new optically transparent focused P(VDF-TrFE) transducer provides a higher sensitivity, a simpler fabrication process, and an achievement of high NA using more brittle piezoelectric films, which could be useful for enabling new PAM systems for different imaging applications.

II. TRANSDUCER DESIGN AND CONSTRUCTION

Fig. 2 shows the schematic design of the new optically transparent focused P(VDF-TrFE) transducer.

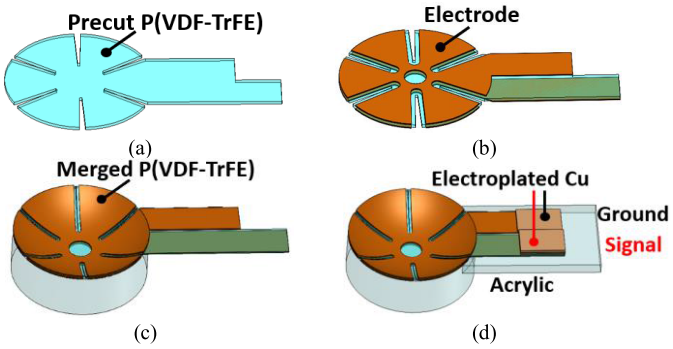

Fig. 3. Fabrication process flow of the optically transparent focused P(VDF-TrFE) transducer. (a) P(VDF-TrFE) precut for fitting into a spherical surface. (b) Electrodes deposition on both sides of P(VDF-TrFE). (c) P(VDF-TrFE) merged into a spherical shape and bonded onto the concave glass lens. (d) Long electrode tail flipping, Cu electroplating on both electrode tails for electrical connections and acrylic attached for electrode support.

The 10-μm-thick P(VDF-TrFE) film (70/30 mol%, Piezotech, France) is precut into a specific pattern and merged into a fit spherical shape after directly laminating onto the curved surface of the concave glass lens (Edmund Optics, USA) with optical epoxy (Epotek 301, Epoxy Technology, USA). The concave glass lens has a diameter of 12.0 mm and a spherical radius of 9.4 mm, corresponding to an acoustic focal length of 9.4 mm and NA of 0.64. The entire P(VDF-TrFE) film is coated with metal electrodes, except that a 2-mm-diameter window at the center is bare for the light to pass through. The P(VDF-TrFE) film at the window is kept for two main reasons. First, optical epoxy can be prevented from overflowing to bond the two lenses together, which makes the convex lens releasing much easier. Second, with the P(VDF-TrFE) film left in the window, the entire P(VDF-TrFE) film becomes more robust to avoid tearing during the fabrication process.

The specific fabrication flow of the new optically transparent focused P(VDF-TrFE) transducer is shown in Fig. 3. First, the P(VDF-TrFE) film is trimmed into a specific pattern for fitting into a spherical surface by a mechanical cutter (Roland DGA, USA) [Fig. 3(a)]. Second, with two shadow masks, chromium (15-nm thickness, 1 Å/s rate) and then copper (400-nm thickness, 2 Å/s rate) layers are e-beam evaporated onto both sides of the P(VDF-TrFE) film [Fig. 3(b)]. The coverage area of the metal electrode around the precut trenches is slightly smaller than the cut patterns to avoid electrical shorting of the two electrodes. Indium–tin oxide (ITO) electrodes are not coated onto the central transparent window to maximize the optical transmittance and to further simplify the fabrication process. The transparent window has little influence on the vibration mode of P(VDF-TrFE) film (dominated by the thickness mode) because the film thickness (10 μm) is much

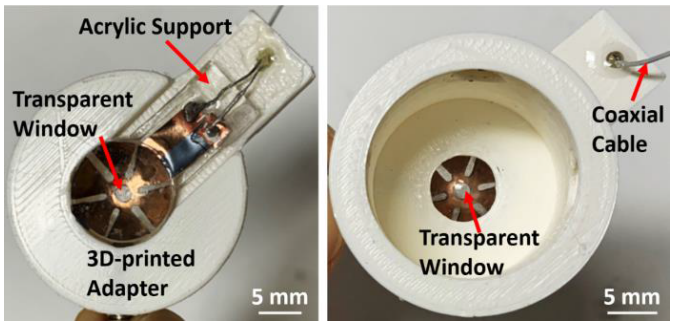

(a) (b)

Fig. 4. Photographs of (a) front and (b) back sides of the prototype optically transparent focused P(VDF-TrFE) transducer mounted on a 3-D printed adapter.

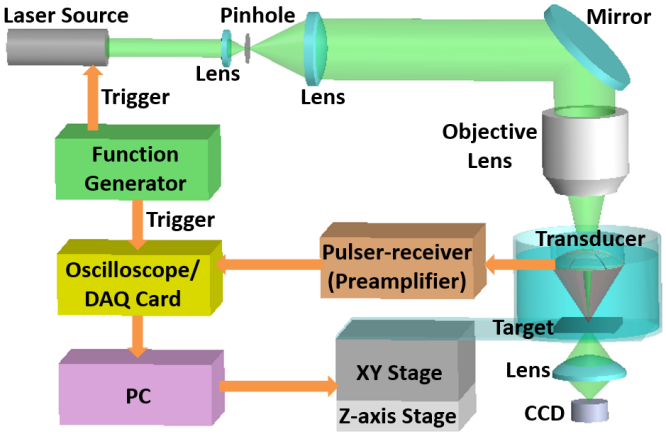

Fig. 5. Experimental setup to characterize the optical, acoustic, and PA imaging performances of the optically transparent focused P(VDF-TrFE) transducer.

smaller than its diameter (12 mm) and the film is firmly bonded onto the concave lens so that other resonant modes are strongly damped. Its acoustic detection sensitivity is not significantly degraded because the transparent window is much smaller than the entire transducer. Third, the metal-coated P(VDF-TrFE) film is merged into a spherical shape and bonded onto the concave surface of the glass lens [Fig. 3(c)] with optical epoxy (density $\rho = 1150$ kg/m^3, sound velocity $c = 2650$ m/s, acoustic impedance $Z = 3.05$ MRayls, Young's modulus $Y = 5.8$ GPa, and optical transmittance $T > 99\%$ @ 382–980 nm [22], [23], [24]). Finally, the copper-coated tail of P(VDF-TrFE) film is flipped and both electrode tails are electroplated with 5-μm-thick Cu to facilitate the electrical connections with a coaxial cable. A piece of acrylic (1 mm thick) is attached to the glass lens to firmly support the electrodes of the transducer [Fig. 3(d)]. A prototype of the fabricated optically transparent focused P(VDF-TrFE) transducer is shown in Fig. 4. The transducer is mounted onto a 3-D printed adapter for the installation onto a microscope objective lens during testing.

III. Transducer Testing and PA Imaging Setup

A testing setup has been built for characterizing the optical, acoustic, and PA imaging performances of the optically transparent focused P(VDF-TrFE) transducer (Fig. 5). A function generator (Keysight Technologies, USA) triggers a Q-switched 532-nm Nd:YAG laser (Elforlight, U.K.) to generate nanosecond (<1.8 ns) laser pulses at a pulse repetition rate (PRR) of 1 kHz. The pulsed laser beam is expanded by a pair of lenses (Thorlabs, USA) and filtered by a 50-μm pinhole (Thorlabs) between them. The expanded laser beam is deflected by a fixed mirror and focused by a 10× optical objective lens (parfocal length = 45 mm and working distance = 6.56 mm) onto the target after passing through the optically transparent focused P(VDF-TrFE) transducer. The excitation region of the target is monitored by a charge-coupled device (CCD) camera in the transmission mode. To achieve efficient acoustic coupling, the target and the front spherical surface of transducer are both submersed in water inside a Petri dish. The Petri dish is placed onto a transparent plate mounted on an XYZ stage, which consists of a computer-controlled X/Y motor stage (Physik Instrumente GmbH and Company KG, Germany) and a manually adjusted Z-axis stage (MPositioning, China). The signal received by the optically transparent focused P(VDF-TrFE) transducer is 39 dB amplified by a preamplifier embedded in the pulser-receiver (Olympus NDT, USA) and sampled by the oscilloscope (Tektronix Inc., USA) or data acquisition (DAQ) card (Alarzar Tech, Canada), which is also triggered by the function generator.

The optical transmittance of the optically transparent focused P(VDF-TrFE) transducer is characterized in air (with the target and Petri dish removed). The average intensity of the laser pulses passing through the transducer is measured with an optical power meter (Thorlabs). The optical power passing through a bare concave glass lens is also measured to serve as the reference for determining the optical transmittance of the focused P(VDF-TrFE) transducer. Ultrasound pulse-echo testing is employed to characterize the acoustic properties of the optically transparent focused P(VDF-TrFE) transducer. A sharp razor blade in water is used as the target, while pulsed laser is turned off. Driven by the pulser-receiver with a PRR of 200 Hz, acoustic pulses are transmitted from the focused P(VDF-TrFE) transducer and incident onto the sharp edge of the blade. The (echo) ultrasound signals scattered from the edge propagate along the inverse path and are detected by the focused P(VDF-TrFE) transducer, preamplified by the pulser receiver, and recorded by the oscilloscope. PAM on different targets is also conducted to investigate the PA imaging performance of the optically transparent focused P(VDF-TrFE) transducer, including lateral resolution, penetration depth, and 2-D mapping of more complex structures. The optical and acoustic foci are first aligned together by adjusting the installation of the transducer on the objective lens to maximize the acoustic detection sensitivity. During imaging, the target is continuously moved by the X/Y stage, while the PA signals are collected by the DAQ card for image reconstruction.

IV. Transducer Testing Results

The optical transmittance is calculated as the ratio of the average optical power after the optically transparent focused P(VDF-TrFE) transducer over that after a bare concave glass lens. Based on the measurement results, the optical transmittance of the optically transparent focused P(VDF-TrFE) transducer is determined to be 88.6% at a 532-nm

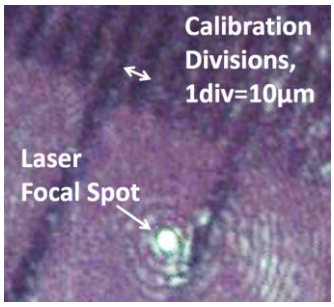

Fig. 6. Laser focal spot size measurement with a calibration glass slide.

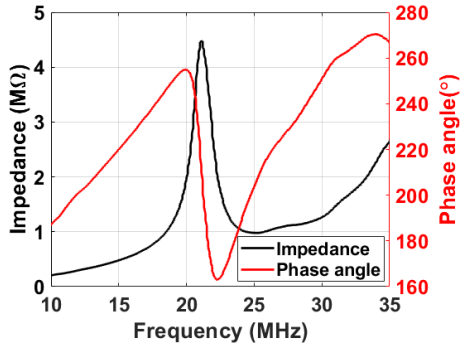

Fig. 7. Measured electrical impedance (black line) and phase angle (red line) spectra of the optically transparent focused P(VDF-TrFE) transducer, indicating the resonant frequency (f_r), antiresonant frequency (f_a), and electromechanical coupling factor (k_{33}) around 20.6 MHz, 21.2 MHz, and 0.26, respectively.

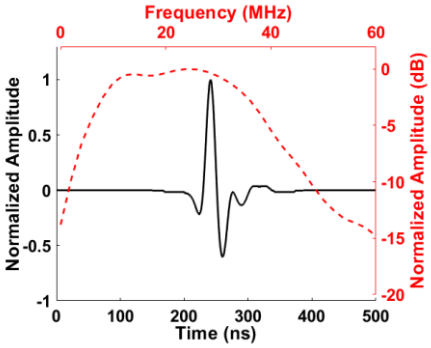

Fig. 8. Representative echo ultrasound signal (in black solid) and its frequency spectrum (in red dashed) of the optically transparent focused P(VDF-TrFE) transducer.

wavelength, which is significantly higher than that (~60%) of ITO-coated PVDF film [11], [12]. This is because the ITO coatings can increase the light reflection due to its high refractive index. The impact on the laser focal spot from the transparent window of the focused P(VDF-TrFE) transducer is characterized with a calibration glass slide (AmScope, USA). After propagating through the objective lens and the optically transparent focused P(VDF-TrFE) transducer, the focal spot of the laser beam is measured to be around 6.5 μm in diameter (Fig. 6). For comparison, the diameter of the laser spot is around 6.0 μm after replacing the transducer with a bare concave glass lens. Therefore, the optically transparent focused P(VDF-TrFE) transducer causes little distortion to the propagation of laser pulses to excite PA signals.

Fig. 7 shows the electrical impedance and phase angle spectra of the focused P(VDF-TrFE) transducer in air, which is measured by electrical impedance spectroscopy (Sciospec

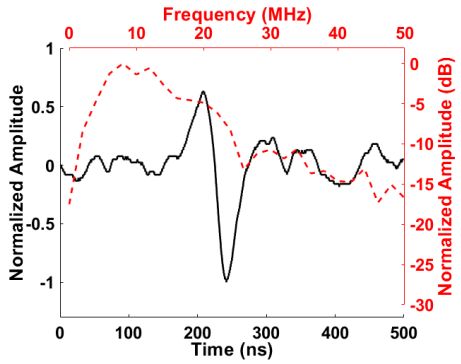

Fig. 9. Representative PA signal (in black solid) from a black tape target and its frequency spectrum (in red dashed).

Scientific Instruments GmbH, Germany). Based on the curve, the transducer resonant frequency (f_r), antiresonant frequency (f_a), and electromechanical coupling factor (k_{33}) are estimated around 20.6 MHz, 21.2 MHz, and 0.26, respectively. f_r is not clear, which is mainly due to the wideband acoustic response of the transducer. Fig. 8 shows a representative ultrasound echo signal (solid black) and its frequency spectrum (dashed red) after fast Fourier transformation (FFT), which indicates a central frequency (f_c) and a BW of 24 MHz (close to that estimated from the electrical impedance curve) and 29 MHz, respectively. The measured f_c and BW of the focused P(VDF-TrFE) transducer are somewhat lower than those of the previous molded PVDF transducer ($f_c \approx 36$ MHz and BW ≈ 44 MHz) [12], which is possibly due to the larger thickness of P(VDF-TrFE) film and also the epoxy layer used for bonding. In addition, the slightly reduced NA (caused by the uncoated transparent window at the center) and less perfect spherical shape of the merged P(VDF-TrFE) film may slightly deteriorate the synchronization of the ultrasound wavefront, which can also contribute to the lower f_c and BW. Based on the measured f_c, BW, and nominal acoustic NA (e.g., 0.64), the acoustic focal spot size, axial resolution, and depth of focus (DOF) of the optically transparent focused P(VDF-TrFE) transducer are estimated to be 122.9, 13.3, and 118.6 μm, respectively. The sensitivity of the P(VDF-TrFE) transducer is characterized by a needle hydrophone (Precision Acoustics, U.K.) with a known sensitivity of 53 nV/Pa. The measured sensitivity of the P(VDF-TrFE) transducer is 6.84 μV/Pa, which is almost six times of that (1.19 μV/Pa) of the previous low-NA PVDF transducer [11]. Fig. 9 shows a representative PA signal (black solid) from a black tape layer as the target and its frequency spectrum (dashed red) after FFT excited by the 100-nJ laser pulse. The frequency spectrum indicates that both f_c and BW of the PA signal are around 10 MHz. f_c is much lower than that (~24 MHz) of the pulse-echo ultrasound signal, which is mainly due to the soft black tape and relatively weak laser intensity, while the wide fractional BW (~100%) is typical for the PA signals from a soft target such as black tape.

V. PA Imaging Results

A. DAQ and Image Reconstruction

For the PAM imaging setup with the optically transparent focused P(VDF-TrFE) transducer, the target is continuously

scanned in a straight line to characterize the lateral resolution and penetration depth, while the target is zigzag moved by the program-controlled *XY* stage for 2-D mapping. The time-domain (A-line) signals are acquired by the DAQ card with 250-MHz sample frequency. Then, the raw A-line signals are processed by digital filters for noise reduction and Hilbert transformation for waveform unipolarization. The B-mode PA images are reconstructed by displaying the processed A-line signals in one line, and the PA amplitude profile and 2-D mapping are projected by the maximum amplitude of the processed A-line signal at each location.

B. Lateral Resolution

The lateral resolution of the PAM imaging setup with the optically transparent focused P(VDF-TrFE) transducer is characterized by scanning a square chromium pattern on the United States Air Force (USAF) resolution target (Thorlabs, USA). The PA amplitude profile across the edge of the chromium pattern is fit by the edge spread function (ESF) to calculate the corresponding line spread function (LSF), which is the derivative of the ESF. The lateral resolution is indicated by the full-width at half-maximum (FWHM) of the corresponding LSF. As shown in Fig. 10(a), the PA lateral resolution is estimated as 6.6 μm, which is close to the measured laser spot size (Fig. 6). For verification, five groups of No. 6 line patterns on the USAF resolution target are also scanned along the white dashed line in Fig. 10(b)]. They can be clearly resolved based on the corresponding cross-sectional PA profile [Fig. 10(b)]. The smallest group of line patterns has a spatial frequency of 114 line pairs/mm (corresponding to an FWHM of 8.78 μm). This result verifies the 6.6-μm PA lateral resolution determined by the LSF of the edge of single chromium pattern.

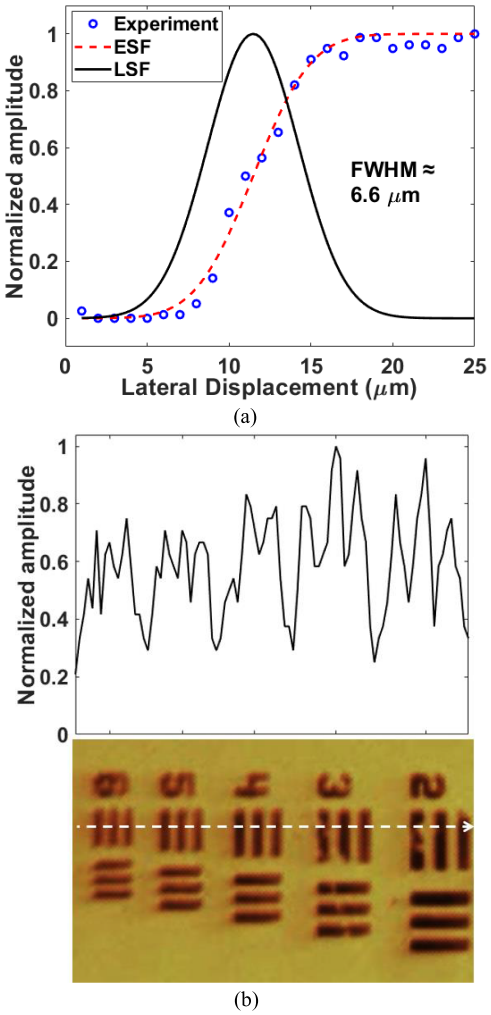

Fig. 10. (a) FWHM of the LSF derived from the fit ESF, indicating the PA lateral resolution around 6.6 μm. (b) Cross-sectional PA profile of the corresponding five groups of No. 6 elements on a resolution target (scanning path indicated by the white dashed line).

C. Penetration Depth

The penetration depth of the PAM imaging setup with the optically transparent focused P(VDF-TrFE) transducer is characterized with a 100-μm-diameter polyimide tubing filled with black ink as the target. Two optically scattering media are tested, including 1% agar (Sigma-Aldrich, USA) phantom and chicken breast tissue. The ink-filled tubing is inserted into the agar phantom and chicken breast tissue at an oblique angle. The PA excitation energy is set to be 200 nJ/pulse. The PAM setup is scanned along the ink-filled tubing for reconstructing a B-mode PA image to show the insertion of the tubing. As shown in Fig. 11(a), the PAM setup can clearly image the tubing down to around 2.1 mm beneath the surface. In the chicken breast tissue, the PAM setup can clearly image the tubing down to around 0.5 mm beneath the surface [Fig. 11(b)]. This shallower depth is mainly due to the stronger optical absorption and scattering in chicken breast tissue than the agar phantom. Some artifacts exist at lateral displacement around 0–1 mm [Fig. 11(b)], which is mainly due to the acoustic reflection inside the glass lens.

D. 2-D Imaging

The 2-D PA imaging capability with the optically transparent focused P(VDF-TrFE) transducer is also explored. A black leaf skeleton with both course (hundreds of micrometers) and fine branches (approximately several tens of micrometers) is laminated on a glass substrate as the imaging target [Fig. 12(a)]. The PA scanning is conducted within an 8 $\times$ 4 mm area and the scanning step size is 8 μm in both directions, which is close to the size of the optical focal spot. The PA excitation energy is set to be 200 nJ/pulse. At each scan point, the PA excitation and reception are repeated 16 times. The captured PA signals are averaged to improve the signal-to-noise ratio (SNR) up to 17.0 dB. The 2-D PAM image [Fig. 12(b)] is reconstructed based on the signal amplitude at each location, which determines the grayscale value of each pixel. Most of the branches are clearly resolved except the finest ones. Further increasing the excitation pulse energy helps to reveal the finer branches, which, however, could increase the chance of structural damage. Due to the weaker signal strength at the edges of the branches, the width of the branches in the PA image appears somewhat smaller than that in the optical micrograph. There are some variations in the signal strength across the reconstructed PA image,

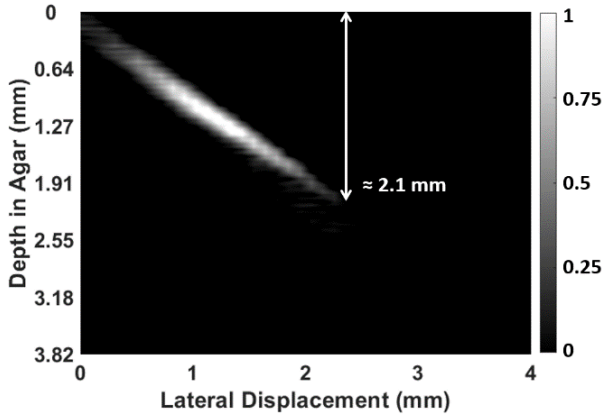

(a)

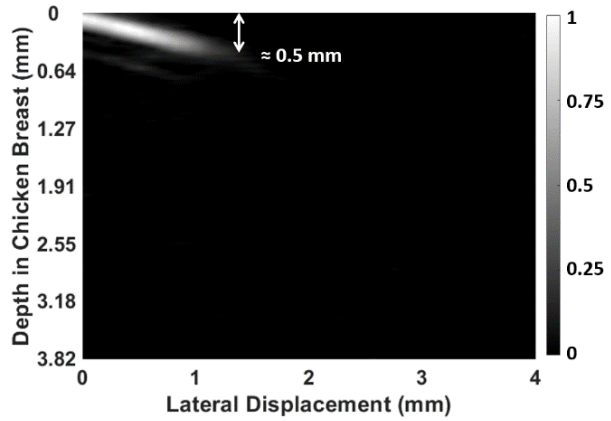

(b)

Fig. 11. B-mode PA images of a 100-μm-diameter polyimide tubing filled with black ink obliquely inserted in (a) 1% agar phantom and (b) chicken breast tissue.

(a)

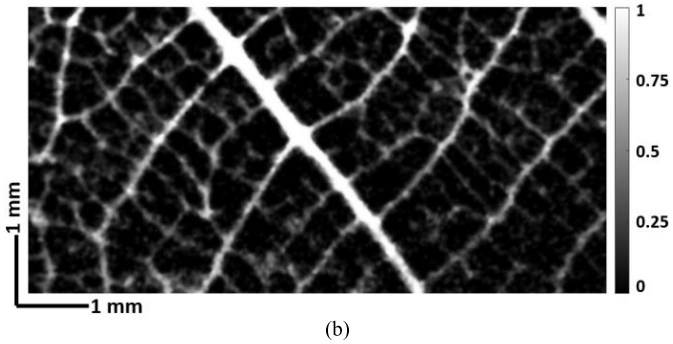

(b)

Fig. 12. (a) Optical photograph and (b) PAM 2-D image of the black leaf skeleton phantom with an area of 8 × 4 mm.

which is caused by the topographic variations of different leaf skeleton branches.

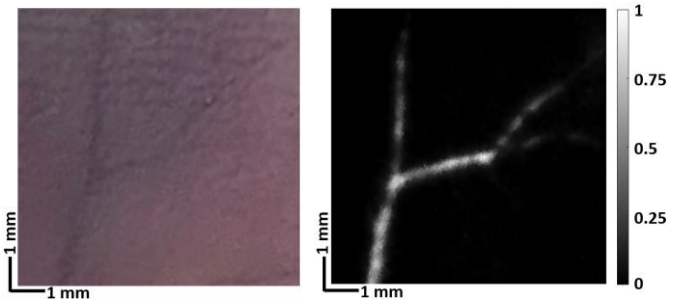

(a) (b)

Fig. 13. (a) Optical photograph and (b) PAM image of the blood vessels in mouse belly with an area of 8 × 8 mm.

The in vivo PAM with the optically transparent focused P(VDF-TrFE) transducer is demonstrated by imaging the mouse belly veins [Fig. 13(a)] with 1.0–1.4 mm depth beneath the skin. The lab animal protocol for this work was approved by the University Laboratory Animal Care Committee of Texas A&M University. The mouse belly hair is gently removed before imaging. The PAM setup is slightly different from that in Fig. 5, where the Petri dish is above the mouse. The bottom of the Petri dish is opened with a square hole and covered by plastic wrap film (thickness $\approx$ 10 μm) to pass the light and PA signals with little attenuation. Ultrasound gel is pasted between the plastic wrap and mouse belly to improve the coupling and remove air bubbles. The PA scanning (500 nJ/pulse) is conducted across an 8 × 8 mm area with a 20-μm scanning step in both directions. As the pulsed laser is focused at 1.2 mm beneath the skin, the surface light fluence is estimated at around 0.88 mJ/cm^2, which is far below the ANSI safety limit (20 mJ/cm^2). Forty scans are repeated at each point to improve the SNR up to 12.3 dB. The PA image [Fig. 13(b)] shows the veins in the mouse belly. Similarly, some variation in the signal strength is caused by the topographic nonuniformity of the mouse skin and various vein depths beneath the skin.

VI. Conclusion

In summary, a new optically transparent focused P(VDF-TrFE) transducer for PAM has been demonstrated, which is fabricated by a new process based on precutting and direct lamination. Compared with the previous fabrication process, it is more sensitive, simpler, and more suitable for mass fabrication and makes it possible to achieve a high NA without stretching the (brittle) piezoelectric film. A prototype P(VDF-TrFE) transducer is fabricated and characterized, and its application in PAM imaging has been demonstrated. The experimental results show that the optically transparent focused P(VDF-TrFE) transducer could be useful for the development of new PAM systems for different imaging applications.

It should be noted that the spherical shape of the laminated P(VDF-TrFE) film can be better defined by optimizing the precut pattern design. The electrode coverage can be enlarged by improving the shadow mask alignment. With these enhancements, the effective aperture and acoustic performance of the focused P(VDF-TrFE) transducer can be further improved. A customized preamplifier with optimal impedance

matching and low noise level can also be used to further boost up the SNR [25].

ACKNOWLEDGMENT

The authors thank the Comparative Medicine Program (CMP) at Texas A&M University, College Station, TX, USA, for assistance in animal handling.

REFERENCES

[1] L. V. Wang, *Photoacoustic Imaging and Spectroscopy*. Boca Raton, FL, USA: CRC Press, 2017.
[2] L. V. Wang and J. Yao, "A practical guide to photoacoustic tomography in the life sciences," *Nature Methods*, vol. 13, no. 8, pp. 627–638, Aug. 2016.
[3] J. Park et al., "Quadruple ultrasound, photoacoustic, optical coherence, and fluorescence fusion imaging with a transparent ultrasound transducer," *Proc. Nat. Acad. Sci. USA*, vol. 118, no. 11, Mar. 2021, Art. no. e1920879118.
[4] S. Park, S. Kang, and J. H. Chang, "Optically transparent focused transducers for combined photoacoustic and ultrasound microscopy," *J. Med. Biol. Eng.*, vol. 40, no. 5, pp. 707–718, Oct. 2020.
[5] H. Chen et al., "A high sensitivity transparent ultrasound transducer based on PMN-PT for ultrasound and photoacoustic imaging," *IEEE Sensors Lett.*, vol. 5, no. 11, pp. 1–4, Nov. 2021.
[6] Z. Li, A. K. Ilkhechi, and R. Zemp, "Transparent capacitive micromachined ultrasonic transducers (CMUTs) for photoacoustic applications," *Opt. Exp.*, vol. 27, no. 9, pp. 13204–13218, 2019.
[7] H. Li, B. Dong, Z. Zhang, H. F. Zhang, and C. Sun, "A transparent broadband ultrasonic detector based on an optical micro-ring resonator for photoacoustic microscopy," *Sci. Rep.*, vol. 4, no. 1, pp. 1–8, Mar. 2014.
[8] Z. Yan and J. Zou, "Large-scale surface-micromachined optical ultrasound transducer (SMOUT) array for photoacoustic computed tomography," *Opt. Exp.*, vol. 30, no. 11, pp. 19069–19080, 2022.
[9] E. Zhang, J. Laufer, and P. Beard, "Backward-mode multiwavelength photoacoustic scanner using a planar Fabry–Pérot polymer film ultrasound sensor for high-resolution three-dimensional imaging of biological tissues," *Appl. Opt.*, vol. 47, no. 4, pp. 561–577, 2008.
[10] R. Shnaiderman, G. Wissmeyer, O. Ülgen, Q. Mustafa, A. Chmyrov, and V. Ntziachristos, "A submicrometre silicon-on-insulator resonator for ultrasound detection," *Nature*, vol. 585, no. 7825, pp. 372–378, Sep. 2020.
[11] C. Fang, H. Hu, and J. Zou, "A focused optically transparent PVDF transducer for photoacoustic microscopy," *IEEE Sensors J.*, vol. 20, no. 5, pp. 2313–2319, Mar. 2020.
[12] C. Fang and J. Zou, "Acoustic resolution photoacoustic microscopy (AR-PAM) based on an optically transparent focused transducer with a high numerical aperture," *Opt. Lett.*, vol. 46, no. 13, pp. 3280–3283, 2021.
[13] Y.-Y. Choi et al., "Vertically aligned P(VDF-TrFE) core-shell structures on flexible pillar arrays," *Sci. Rep.*, vol. 5, no. 1, Jun. 2015, Art. no. 10728.
[14] A. Vinogradov and F. Holloway, "Electro-mechanical properties of the piezoelectric polymer PVDF," *Ferroelectrics*, vol. 226, no. 1, pp. 169–181, Apr. 1999.
[15] H. Ohigashi, K. Koga, M. Suzuki, T. Nakanishi, K. Kimura, and N. Hashimoto, "Piezoelectric and ferroelectric properties of P (VDF-TrFE) copolymers and their application to ultrasonic transducers," *Ferroelectrics*, vol. 60, no. 1, pp. 263–276, Oct. 1984.
[16] F. S. Foster, K. A. Harasiewicz, and M. D. Sherar, "A history of medical and biological imaging with polyvinylidene fluoride (PVDF) transducers," *IEEE Trans. Ultrason., Ferroelectr., Freq. Control*, vol. 47, no. 6, pp. 1363–1371, Nov. 2000.
[17] Z. Y. Cheng, H. Xu, T. X. Mai, T. M. Chung, Q. M. Zhang, and R. Y. Ting, "P(VDF-TrFE)-based electrostrictive co/ter-polymers and their device performance," *Proc. SPIE*, vol. 4329, pp. 106–116, Jul. 2001.
[18] W. H. Liew, M. S. Mirshekarloo, S. Chen, K. Yao, and F. E. H. Tay, "Nanoconfinement induced crystal orientation and large piezoelectric coefficient in vertically aligned P(VDF-TrFE) nanotube array," *Sci. Rep.*, vol. 5, no. 1, pp. 1–7, May 2015.
[19] K. K. Shung, J. M. Cannata, and Q. F. Zhou, "Piezoelectric materials for high frequency medical imaging applications: A review," *J. Electroceram.*, vol. 19, no. 1, pp. 141–147, Oct. 2007.
[20] H. L. W. Chan et al., "Polarization of thick polyvinylidene fluoride/trifluoroethylene copolymer films," *J. Appl. Phys.*, vol. 80, no. 7, pp. 3982–3991, Oct. 1996.
[21] P.-H. Ducrot, I. Dufour, and C. Ayela, "Optimization of PVDF-TrFE processing conditions for the fabrication of organic MEMS resonators," *Sci. Rep.*, vol. 6, no. 1, pp. 1–7, Jan. 2016.
[22] J. Yu and A. Kidane, "Acoustic properties of composites containing multiple heterogeneities: Micromechanics modelling," *Int. J. Theor. Appl. Multiscale Mech.*, vol. 2, no. 4, pp. 271–286, 2013.
[23] M. Osman et al., "A novel translucent ultrasound transducer approach for dual-modality ultrasound and photoacosutic imaging," *Proc. SPIE*, vol. 11960, pp. 331–337, Mar. 2022.
[24] *Epoxy Technology, Inc. Epotek 301 Technical Data SheetEpoxy Technology*. Accessed: Feb. 2021. [Online]. Available: https://www.epotek.com/docs/en/Datasheet/301.pdf
[25] Y. H. Liu et al., "Sensitive ultrawideband transparent PVDF-ITO ultrasound detector for optoacoustic microscopy," *Opt. Lett.*, vol. 47, no. 16, pp. 4163–4166, 2022.

Cheng Fang (Graduate Student Member, IEEE) received the B.E. degree in information engineering from Zhejiang University, Hangzhou, Zhejiang, China, in 2011, and the M.Eng. degree in electrical engineering from Texas A&M University, College Station, TX, USA, in 2013, where he is currently pursuing the Ph.D. degree.

His research interests include microfabrication technology, near-distance sensing systems, and photoacoustic (PA) imaging devices and systems.

Zijie Zhao received the B.E. degree in measurement and control technology and instrumentation from the Huazhong University of Science and Technology, Wuhan, Hubei, China, in 2014, and the M.Eng. degree in optical engineering from Beihang University, Beijing, China, in 2018. He is currently pursuing the Ph.D. degree in electrical engineering with Texas A&M University, College Station, TX, USA.

His research interests include photoacoustic (PA) manipulation, PA measurement, and PA imaging devices and systems.

Jie Fang received the B.E. degree in electronic science and technology from Southeast University, Nanjing, Jiangsu, China, in 2019, and the M.S. degree in electrical engineering from Texas A&M University, College Station, TX, USA, in 2022.

His research interests include microfabrication technology, ultrasonic transducers, and mixed-signal integrated circuit (ICs).

Jun Zou (Senior Member, IEEE) received the Ph.D. degree in electrical engineering from the University of Illinois at Urbana–Champaign, Champaign, IL, USA, in 2002.

In 2004, he joined the Department of Electrical and Computer Engineering, Texas A&M University, College Station, TX, USA, where he is currently a Full Professor and directs the Micro Imaging and Sensing Devices and Systems (MISDS) Laboratory. His current research interests include the development of micro and nano opto-electromechanical devices and systems for biomedical imaging, robotics, and artificial intelligence applications.

Dr. Zou is a Senior Member of the Society of Photo-Optical Instrumentation Engineers (SPIE).